Magnetic structure of MFe_4Al_8, M = Y and U: a comparative study

2008 J. Phys.: Condens. Matter 20 075224

(http://iopscience.iop.org/0953-8984/20/7/075224)

J. Phys.: Condens. Matter **20** (2008) 075224 (9pp) doi:10.1088/0953-8984/20/7/075224

Magnetic structure of MFe_4Al_8, M = Y and U: a comparative study

C Cardoso[1], T Gasche[2,3] and M Godinho[2,4]

[1] CFC, Physics Department, University of Coimbra, 3004-516 Coimbra, Portugal
[2] Centro de Física da Matéria Condensada—Universidade de Lisboa, Campo Grande, Edifício C8, 1749-016, Lisboa, Portugal
[3] CINAMIL Laboratório de Física, Academia Militar, Lisboa, Portugal
[4] Departamento de Física, Faculdade de Ciências, Universidade de Lisboa, Campo Grande, Edificio C8, 1749-016, Lisboa, Portugal

E-mail: cmcardoso@teor.fis.uc.pt

Received 22 October 2007, in final form 10 January 2008
Published 31 January 2008
Online at stacks.iop.org/JPhysCM/20/075224

Abstract

In this paper we present a comparative analysis of the isostructural compounds MFe_4Al_8, with M = Y and U. These compounds have different magnetic ground state structures: a cycloid spin spiral in the case of YFe_4Al_8 and a canted structure in the case of the actinide compound. Model calculations show that it is the presence of a strong spin–orbit coupling in the actinide compound that leads to a magnetic configuration with symmetry properties that differ from the YFe_4Al_8 cycloid structure. Furthermore we show that in the absence of spin–orbit coupling, the U compound would have the same spin spiral as the Y compound. A further analysis for two actinide compounds, UFe_4Al_8 and $NpFe_4Al_8$, point to similar magnetic ground state structures; however the actinides play different roles in the magnetisms of the two compounds. Despite their differences, all three magnetic structures can be seen as deviations from the type G antiferromagnetic structure.

New calculations for UFe_4Al_8 permit a clarification of previous computational studies, and we present, within a simplified model, an analysis of the Fe–Fe exchange interactions for YFe_4Al_8 and UFe_4Al_8, calculated within the frozen magnon approximation.

1. Introduction

The compounds MFe_4Al_8, where M is a rare earth or an actinide, and the semi-ordered alloys MFe_xAl_{12-x} which form in a large range of compositions, have large magnetic moments and anisotropic magnetic properties. The combination of a large range of compounds with unusual magnetic properties and the possibility of technological applications has focused the interest of a large number of researchers in this area. A previous theoretical study of the UFe_xAl_{12-x} [1, 2] has analysed the role of the variation of the Fe content within the U compound, in this paper we present a comparative study of the role of the M element for the actinide U and the rare earth Y. Further comparisons between the U and the Np isostructural compounds show the similarities between the actinide compounds and reforce the common points, and the differences, between the actinide and rare earth compounds of this series.

In the majority of these compounds both the M and the Fe sublattices are magnetic and both the actinide and rare earth compounds of the MFe_4Al_8 series show complex ground state magnetic configurations. The large variety of magnetic configurations ranges from spin spirals [3–5], to noncollinear antiferromagnetic and ferromagnetic structures [6, 7], or even spin modulated configurations [8]. The magnetic structures, partially determined by the level of localization and hybridization of the wave functions, are also constrained by symmetry, in this case imposed by the crystal structure and the presence of spin–orbit coupling, with different effects for the actinides and the rare earths compounds.

UFe_4Al_8 is a good example of this complexity and its unusual physical properties have been the focus of attention for the last two decades [6, 9–17]. Unlike the RFe_4Al_8 (R = magnetic rare earth) compounds, where the ordering of the rare earth and iron magnetic moments develop at different temperatures [4], in UFe_4Al_8 only one

transition temperature, involving the two magnetic sublattices, is observed [6]. Neutron diffraction experiments on a stoichiometric single crystal report Fe moments aligned along the a (or the equivalent b) axis of the tetragonal structure with a slightly canted antiferromagnetically structure and the uranium moments ferromagnetically aligned in the (a, b) plane and almost perpendicular to the iron moments [6]. Therefore, this structure has a ferromagnetic contribution from the uranium atoms (0.47 μ_B/U), and a weak ferromagnetic contribution from the iron sublattice (0.3 μ_B/Fe). Magnetization measurements on single crystal samples have confirmed the a and b as the easy magnetization axes [16]. A relativistic band structure calculation of UFe_4Al_8 shows that the magnetism at the uranium atoms is induced by the of the iron sublattice [11] and is a result of the hybridization between the itinerant Fe 3d and U 5f electrons. $NpFe_4Al_8$ has been less studied than its isostructural U compound [18–22]. Early studies report that Np and Fe moments order along the c axis at close temperatures, 115(10) K and 130(10) K, with, respectively, ferro and antiferromagnetic configurations [18, 19]. Subsequent studies led to the proposal of a spin-glass state at low temperatures [20]. Later experimental studies show that $NpFe_4Al_8$ has a magnetic behaviour that is similar to that of UFe_4Al_8 and a parallel theoretical study showed that the two magnetic sublattices, although coupled by hybridization, can order independently in this compound [22].

Studies of the RFe_4Al_8 series in the late 1970s determined antiferromagnetic interactions for the Fe sublattice with ordering temperatures between 90 and 200 K [23–25]. The reported ordering temperatures of the magnetic rare earth atoms are lower than 50 K, which is explained by antiferromagnetic structure of the Fe sublattice and the high symmetry of the 2a sites, occupied by the rare earths. Later, polycrystalline samples of MFe_4Al_8, M = La, Ce, Lu, Y [3] and Tb [26], were reported to order between 130 and 200 K with distinct types of spiral structures requiring two sets of wavevectors for their description with Fe moments close to 2 μ_B per atom. YFe_4Al_8 was found to order at around 185 K with the Fe moments forming two cycloids in the a–b plane with propagation vector $\mathbf{q} = \frac{2\pi}{a}(0.135, 0.135, 0)$ [3] and a phase difference of $\pm 140°$. In the case of YFe_4Al_8, Y is non-magnetic and therefore the Fe moments form the only magnetic lattice. The Fe moments order in a spin spiral with propagation vector along [110] [3, 8]. Mössbauer studies on YFe_4Al_8 show a gradual ordering of the Fe lattice and suggest a negligible effect of the rare earth on the Fe sublattice [27, 28]. The reported experimental values for the Fe magnetic moment in YFe_4Al_8 vary from 0.7 μ_B/Fe, determined by Mössbauer spectroscopy [27], to 2.1 μ_B/Fe, measured by neutron diffraction [3]. Both values are far from the values determined for similar compounds: 1.3 μ_B for $LuFe_4Al_8$ [8], for example.

Deviations in the samples' stoichiometry and the drastic differences in the magnetic properties of compounds with similar compositions, along with the complex magnetic structures, explain the large range of experimental results. Previous theoretical studies have contributed to a fuller understanding of the experimental data [11, 22, 29], in the present work the theoretical study will be expanded to allow a direct comparison of the compounds in question.

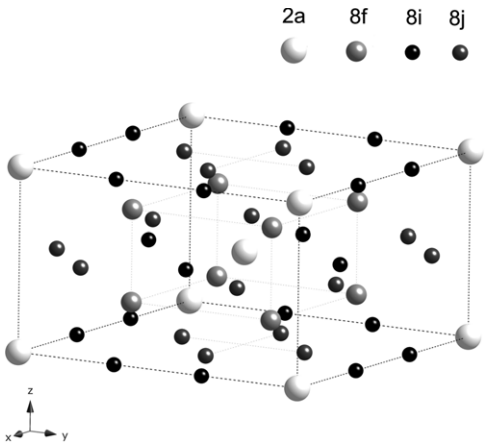

Figure 1. $ThMn_{12}$ crystal structure.

1.1. Symmetry properties

These compounds crystallize in a body centred tetragonal $ThMn_{12}$ type structure, shown in figure 1 [30]. The actinide or rare earth atoms occupy the 2a sites while Fe occupies the 8f sublattice and the 8j and 8i sites are occupied by Al [31].

The symmetry of UFe_4Al_8 and $NpFe_4Al_8$ was described in [11, 22] and that of rare earth compounds, for example YFe_4Al_8 with $ThMn_{12}$ type structures was studied in [32]. The differences between the actinide compounds and YFe_4Al_8 is related to the spin–orbit coupling. In the actinide compounds, the spin–orbit coupling of the itinerant 5f electrons plays an important role coupling the space and spin coordinates and decreases the symmetry of the system. In the case of the rare earth compounds, there are no itinerant f functions, and this symmetry reduction does not occur.

As discussed by Sandratskii [33], the absence of a strong spin–orbit coupling in the itinerant electrons permits the development of a spin spiral. However for the actinide compounds the spin–orbit coupling of the itinerant 5f electrons does not permit the formation of a spin spiral: the crystal symmetry determines a magnetic structure where the Fe moments deviate from a collinear type G antiferromagnet, developing a component parallel to the actinide moment [11].

In YFe_4Al_8 the fact that the spin and space coordinates are decoupled permits the existence of a spin spiral. The spin spiral structures are generated by a symmetry operation consisting of a spatial translation and a spin rotation. The magnetic structure determined by neutron diffraction is described as a cycloid structure with a propagation vector $\mathbf{q} = \frac{2\pi}{a}(\tau, \tau, 0)$ and the Fe moments on the a–b plane [3]. The compounds with a wavevector of this type, belonging to $Imm2$ the space group, have point group components: $C_2^{xy}\nu = \{1, 2_{xy}, m_{-xy}, m_z\}$. Since the propagation vector is not invariant under a four fold rotation, the Fe atoms, within equivalent crystal sites, are split into two magnetic sublattices. For each site the magnetic

moment may be described through vectors given by:

$$m(\mathbf{r}) = M(\mathbf{e}_1 \cos(\mathbf{q}\cdot\mathbf{r} + \theta_i) + \mathbf{e}_2 \sin(\mathbf{q}\cdot\mathbf{r} + \theta_i)). \quad (1)$$

This model corresponds to a cycloid structure for the two Fe lattices with the same chirality and the magnetic moments on the (001) plane. However there can be a nonzero phase, represented by θ_i, with $i = 1, 2$, with a value not determined by symmetry. Additional physical constraints are required to determine the phase value.

1.2. Previous results

Previous theoretical studies of YFe_4Al_8 [29] consist of self-consistent calculations of the density of states and magnetic moments and the comparison of the total energy of different magnetic configurations, calculated with the use of the force theorem. The magnetic moment is similar for all the studied magnetic configurations: as expected Y has negligible magnetic moment and the Fe moment is 1.3 μ_B per atom. The calculated Fe moment is close to the experimental values for similar compounds, and is within the range of the large variety of values reported for YFe_4Al_8, ranging from 0.7 to 2.1 μ_B/Fe. Comparison of several cycloid structures with different wavevectors along the [110] direction, permitted the determination of the lowest energy magnetic configuration, a cycloid with a propagation vector $\mathbf{q} = \frac{2\pi}{a}(0.85, 0.85, 0)$. The value $\tau = 0.85$ is very different from the neutron diffraction value, $\tau = 0.135$ [3], however the reinterpretation of the magnetic structure by considering only one Fe sublattice (which means that the angle between the two iron sublattices is given by $\beta = \mathbf{q}\cdot(\mathbf{r}_3 - \mathbf{r}_1)$), with $\mathbf{q} = \frac{2\pi}{a}(0.85, 0.85, 0)$ leads to an angular relation between the Fe moments similar to that proposed to fit neutron diffraction. In this way there is no need for a second Fe sublattice to describe the magnetic structure.

The magnetic structure of UFe_4Al_8 was determined by neutron diffraction [6]. It consists of a ferromagnetic U lattice and a noncollinear antiferromagnetic Fe lattice. The two lattices are both in the *a*–*b* plane but their moments are almost orthogonal. The angle between the U and Fe moments is 74°. The results of density functional theory calculations [11] in general reproduce well the experimental results. However the U moment is underestimated and the calculated angle between the U and Fe moments is 82°. The study shows also that the orbital polarization correction (OPC) as applied in [34] does not improve the calculated results. For small values of this correction, the U moment decreases and there is an increase in the angle between the U and Fe lattices. If the correction is increased to 1 mRyd, there is a sudden increase of the U moment to 2 μ_B and the angle between the two lattices decreases to 40°. This is one of the problems that will be analysed in the present calculations.

The previous band structure calculations for $NpFe_4Al_8$ confirm the tentative conclusions of the experimental measurements which point to a neptunium moment aligned along one of the crystal axes of the *a*–*b* plane and iron moments forming a noncollinear structure in the same plane [22]. The magnetic structure is similar to UFe_4Al_8: the Np sublattice has a ferromagnetic structure along one of the basal plane axes and the Fe lattice is canted by 13° relatively to the Np moments with an antiferromagnetic projection perpendicular to these moments. This angle should be compared with the 74° angle between the U and Fe moments in UFe_4Al_8, where both elements contribute to the ferromagnetic component. In the Np analogue the magnetic moment direction may be reversed, depending on the magnitude of the orbital and spin contributions. The computational study of $NpFe_4Al_8$ showed a relation between the two magnetic lattices, Fe and the actinide, that is different from UFe_4Al_8. Contrarily to that which happens in UFe_4Al_8 if the Fe lattice is constrained to a null moment, Np keeps a significant moment. When the Np moments are kept null the Fe moments change their alignment to a direction almost perpendicular to their previously direction, close to the type G antiferromagnetic configuration. The inclusion of an OPC term increases significantly the Np orbital moment.

2. Calculation method

The calculations, based on density functional theory, with the von Barth–Hedin parameterization for the local density approximation, were performed using the augmented spherical waves method modified to account for the spin spiral structures as described in [33, 35]. The magnetic moment and density of states were determined by self-consistent calculations, constraining the compounds to several magnetic configurations. The number of reciprocal lattice points in the irreducible part of the Brillouin zone was $10 \times 10 \times 10$. Convergence with respect to the number of reciprocal points was confirmed with 4207 k points. The variation of the magnetic moment is less than 0.001 μ_B/atom. The energy is more sensitive, varying by 0.1 mRyd. Therefore the total energy of each magnetic configuration was determined using a method which is more numerically stable, the magnetic force theorem [36], with 1000 reciprocal lattice points in the Brillouin zone. The eigenvalue sum was calculated at 0 K and at 100 K, the latter using the Fermi–Dirac distribution and taking care to calculate the exact chemical potential; these results differ by less than 0.05 mRyd and do not change the positions of the maxima and minima. Two series of calculations with different initial charge densities resulted in similar results, with deviations smaller than 0.06 mRyd.

One of the problems of the spin spiral calculations is the apparent loss of translational symmetry due to the rotation of the magnetic moments. However in the absence of spin–orbit coupling, i.e. with a scalar-relativistic Hamiltonian, it is possible to use spin-space groups and the corresponding generalized Bloch theorem [37, 38]. This makes it unnecessary to use a super-cell in the calculation of a spin spiral without spin–orbit coupling.

The case of a spin spiral with strong spin–orbit coupling is more complicated as the spin–orbit term does not commute with the translation along a spin spiral: in other words the coupling between the spin and the lattice depends on the relative orientation between them; advancing along a spin spiral from one atom to the next the contribution of the spin–orbit coupling to the Hamiltonian varies as a function

of the spin orientation, *and is not constant from atom to atom*. One way of solving this problem would be to perform super-cell calculations, as used to analyse spin spirals in US [39], however here we used a *frozen spin–orbit coupling* approximation, considering that all of the atoms along the spin spiral have the same spin–orbit coupling. The actual value of the spin–orbit coupling depends on the relative orientation of the spin moment of the atom used in the calculations. Tests, presented in the following section, confirm that this approximation is valid for these compounds.

Using the fact that the electronic and magnetic timescales are different, it is possible treat the magnon excitations within an adiabatic approximation [40]. This approximation neglects the magnetization precession due to the spin wave, assuming that the magnon energy is small when compared with the band widths and the exchange energies of the system. The procedure we used consists in calculating the variations of the total energy for magnetic configurations in which the magnetic moments with different directions, simulating the thermal fluctuations of the moment orientation and neglecting any sort of Stoner fluctuations. Within the frozen magnon approximation this corresponds to choosing static spin spiral configurations described by a wavevector $\mathbf{q}$ and an angle θ, the polar angle that describes the atomic magnetic moments, see for example [33].

The energy of the system can be written as a function of the spin spiral parameters:

$$E_q(\theta) = E_0(\theta) - \frac{\mathrm{sen}^2\theta}{2} J_q \tag{2}$$

where E_0 does not depend on $\mathbf{q}$ and J_q is the Fourier transform of the exchange parameters between atom pairs. Using J_q the excitation energies of the spin waves can be estimated:

$$\omega_q = \frac{4}{M}\left[J_0 - J_q\right] = \frac{8}{M\mathrm{sen}^2\theta}\left[E_q(\theta) - E_0(\theta)\right] \tag{3}$$

where M is the atomic moment. Performing the inverse Fourier transform:

$$J_{0j} = \frac{1}{N}\sum_{\mathbf{q}} J_q \mathrm{e}^{-\mathrm{i}\mathbf{q}\cdot\mathbf{R}_{0j}} \tag{4}$$

the Curie temperature can be calculated within the mean field approximation:

$$k_\mathrm{B}T_\mathrm{C} = \frac{2}{3}\sum_{j\neq 0} J_{0j} = \frac{M}{6\mu_\mathrm{B}}\frac{1}{N}\sum_{\mathbf{q}}\omega_q. \tag{5}$$

All the calculations presented in this paper follow the implementation described in [41] with $\theta = 30°$. The magnon energies were estimated only for the acoustic branch since they correspond to the lower temperatures.

3. Results and discussion

3.1. UFe_4Al_8

In order to clarify some properties of the compound we repeated the computational study of UFe_4Al_8. We started the calculations by the study of the dependence of the U moment with its Wigner–Seitz radius. The magnetic moment, within the atomic sphere approximation (ASA), should not be sensitive to the Wigner–Seitz radius. We performed several calculations with the U moments aligned perpendicular to an antiferromagnetic Fe lattice, in which the relative Fe and U Wigner–Seitz radii were modified, maintaining a constant lattice volume. The results are summarized in table 1. The Fe magnetic moment does not vary however the U spin moment changes from 0.1 to 1.2 μ_B/U, as the Wigner–Seitz deviates from 3.50 au. This radius corresponds to the lower charge transfer for the U atom and is the value used in the calculations that follow. Below we will relate the instability of the U magnetic moment with the shape of the density of states.

Table 1. Spin and orbital magnetic moments of U, calculated for UFe_4Al_8 with different Wigner–Seitz radii. The unit cell volume was kept constant. In the second column is tabled the charge of the U atom in electrons.

U radius (au)	Charge (e)	m_spin (μ_B/U)	m_orb (μ_B/U)
3.45	-1.17×10^{-1}	−1.19	1.71
3.50	1.3×10^{-2}	−0.08	0.21
3.52	1.4×10^{-2}	−0.12	0.29
3.59	2.7×10^{-1}	−1.24	1.79

The density of states calculated for the paramagnetic state is shown in figure 2. The high Fe density of states at the Fermi level leads to a large moment in the magnetic state. The U density of states shows a maximum slightly above the Fermi level but with a local minimum exactly at E_F. Its critical location explains the large range of values for the U moment strongly dependent on the Wigner–Seitz radius, since a slight deviation in energy results in a large variation of the density of states at the Fermi level. The two maxima on the density of states are separated by 0.05 Ryd, which gives an estimate of the spin–orbit coupling splitting. The density of states was also computed for a magnetic configuration with the U moments ordering ferromagnetically and aligned perpendicular to the Fe moments that were constrained to a type G antiferromagnetic order (figure 3). The Fe density of states shows a spin splitting of 0.1 Ryd, with maxima 0.05 Ryd above and below E_F leading to a magnetic moment of 1.3 μ_B/Fe. The U has a smaller splitting, with the main maxima above E_F.

We also determined the ground state configuration using the *magnetic force theorem* [36]. The method consisted in comparing the total energy of different magnetic configurations. We started with the configurations described above and varied the canting angle of the Fe lattice ending in a collinear ferromagnetic structure. In figure 4 the total energy is plotted as a function of the angle between the Fe and U magnetic lattices. The ground state structure corresponds to an angle of 85° which compares well with the 82° reported previously [11]. The small difference is due to the fact that the previously reported value was calculated using a self-consistent variational method for the energy minimization whereas the present canting value was obtained via the force theorem.

A previous study of UFe_4Al_8 concluded that the orbital polarization correction does not improve the calculated

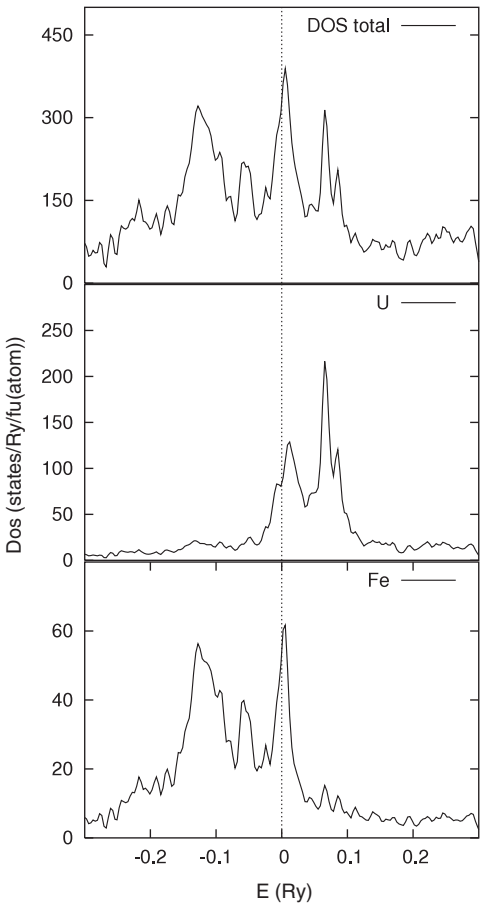

Figure 2. Density of states calculated for the paramagnetic state of UFe_4Al_8 for $r_{WS} = 3.50$ au. The total density of states is given for an entire unit formula and the partial density of states of U, Fe and Al are given for one atom. The Fermi level corresponds to $E = 0$.

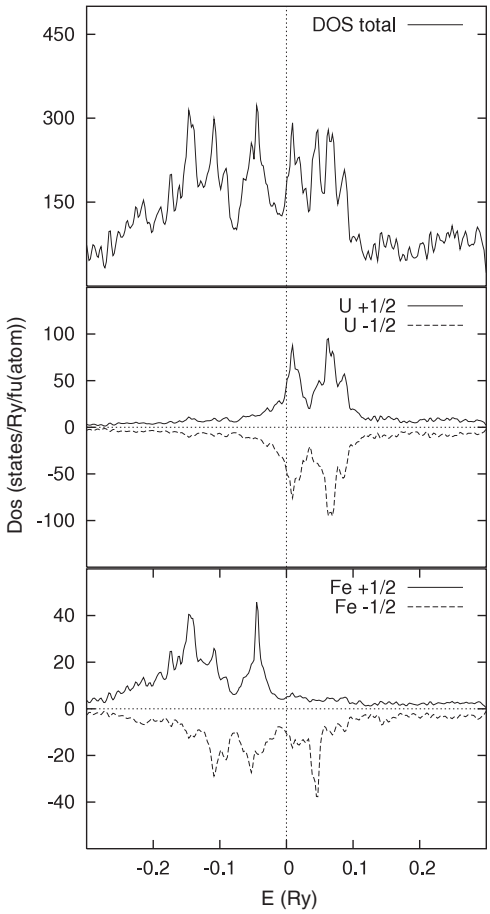

Figure 3. Density of states calculated for a ferromagnetic configuration of U with the moment along **a** and an antiferromagnetic type G configuration of the Fe lattice along **b**. The total density of states is given for an entire unit formula and the partial density of states are given for one atom. The Fermi level corresponds to $E = 0$.

results [11]. To understand this peculiar behaviour we repeated the calculation. Hund's second rule was modelled by adding a term to the Hamiltonian of the form $H_{OP} = I_{OP}E^3Lm_l$ as applied in [34]. This corresponds to a splitting of the m_l states by an energy given by the OPC parameter in mRyd. This correction was applied only to the U f states. In order to better understand the effect of the OPC correction we varied the value of the Racah parameter from 0.01 to 5 mRyd, including the self-consistent value, 2.3 mRyd. The magnetic structure was constrained to a ferromagnetic ordering of the U moments and a type G antiferromagnetic configuration for the Fe lattice, with the moments perpendicular to the U moments.

Two series of calculations were carried out starting from two different U charge densities which converged to two different local minima with different U moments. For some of the values of the orbital polarization correction splitting, it is possible to distinguish the metastable solution from the lower energy configuration. The results obtained in the present study are summarized in table 2. This instability of the U moment can be explained by the same arguments used in the case of the variation of the Wigner–Seitz radii. Within each series the U moment increases, as expected, with the increase of the orbital polarization correction splitting. For an orbital polarization correction of 0.01 mRyd, the lower

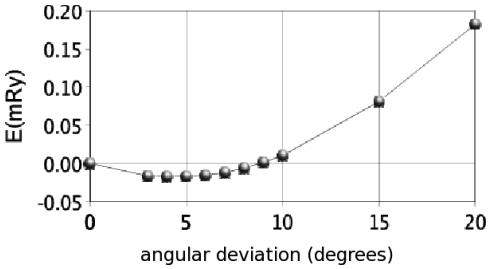

Figure 4. Energy differences of configurations with different canting angles for the Fe moments. The angular deviation of the Fe moment relatively to the type G antiferromagnetic configuration, α is given along the horizontal axis. The angle between the U and Fe moments is given by $\theta = 90° - \alpha$.

moment configuration is 4 mRyd lower than the other state and for an orbital polarization correction of 0.5 mRyd, the difference is already 10 mRyd; however for a orbital splitting of 1 mRyd, the two states present similar total energies, within the accuracy of the calculations. Calculations started with the first charge density and R = 2 mRyd converge to the high spin values. The Racah parameter of 2.3 mRyd corresponds to the

Table 2. U spin, orbital and total moments in UFe_4Al_8—1st and 2nd series of results (depending on initial charge density). The orientation of the magnetic moments was fixed as defined in the text.

Racah parameter (mRyd)	m_{spin} (μ_B/U)	m_{orb} (μ_B/U)	m_{total} (μ_B/U)
0.01	−0.1	0.3	0.2
0.1	−0.6	0.7	0.1
0.5	−0.6	0.9	0.3
1	−0.6	1.0	0.4
0.01	−1.2	1.8	0.6
0.1	−1.3	1.8	0.6
0.5	−1.4	2.2	0.8
1	−1.4	2.5	1.0
2	−1.6	3.1	1.5
2.3	−1.7	3.4	1.7
5	−1.8	4.4	2.6

Table 3. U spin, orbital and total magnetic moments and Fe moments direction calculated self-consistently for UFe_4Al_8 with OPC.

Racah parameter (mRyd)	Fe moments direction	m_{spin} (μ_B/U)	m_{orb} (μ_B/U)	m_{total} (μ_B/U)
1	82.5°	−0.33	0.47	0.17
1	12°	−1.89	2.87	0.98
2.3 (self-c.)	28°	−1.99	3.49	1.50

self-consistently calculated value of the Racah parameter. For all of the calculations, the Fe moment is found to be 1.3 μ_B, with variations less than 0.02 μ_B/Fe.

Four more calculations were performed, in which the direction of the magnetic moments was self-consistently determined, for three reference values of the orbital polarization correction. The results are summarized in table 3. For an orbital polarization correction of 1 mRyd the calculation converges for two different configurations from the two different initial states, showing again the instability of the U moment and the influence of its value in the direction of the Fe moment. The higher the U moment the lower is the angle between the Fe and U magnetic lattices. For an orbital polarization correction splitting of 2.3 mRyd, the two initial densities converged to the same result; there is a significant increase of the U moment and a large decrease on the angle between U and Fe moments, which corresponds to an increase in the magnetization. This is consistent with the results reported in [11].

3.2. Magnetic structure of YFe_4Al_8 and UFe_4Al_8

Calculations for a spin spiral configuration were performed for UFe_4Al_8 also using the *magnetic force theorem*. The same type of cycloids described in section 1.1 were considered, with propagation vectors along [110], of the form $\mathbf{q} = \frac{2\pi}{a}(\tau, \tau, 0)$. The magnetic moments were kept in the basal plane and, initially, no additional phase difference was considered between the U and Fe lattices. Therefore the angle between the atomic moments, θ, is given by the scalar product of the propagation vector and the position vector $\theta = \mathbf{q} \cdot (\mathbf{r}_{Fe} - \mathbf{r}_U)$. In order to understand how spin–orbit coupling affects the magnetic configurations two series of calculations were performed; the first series of spin spiral calculations was performed without the inclusion of spin–orbit coupling, the second series including this term. Since the spin–orbit coupling term depends on the direction of the moment relative to the crystal axis, in a spin spiral it breaks the translational symmetry. Therefore, in the second set of calculations, a *frozen spin–orbit coupling* term was included as described in the previous section.

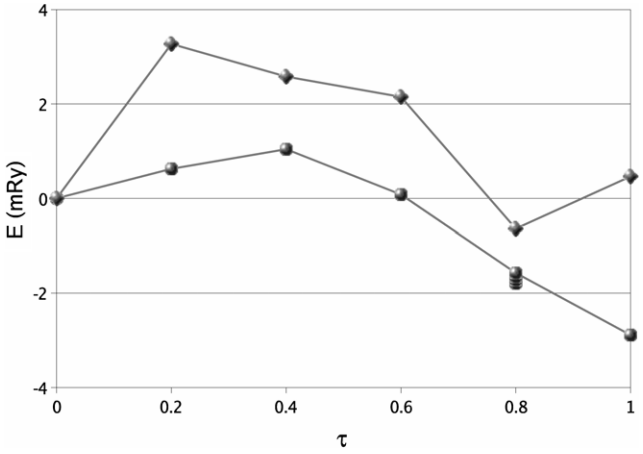

Figure 5. Relative energy for UFe_4Al_8 with a magnetic cycloid with a propagation vector $\mathbf{q} = \frac{2\pi}{a}(\tau, \tau, 0)$: upper (lower) line, not including (including) spin–orbit coupling. The various points for the $\tau = 0.8$ (with spin–orbit coupling) correspond to different initial orientations of the cycloid, as described in the text.

The results plotted in figure 5 show that the lowest energy configuration changes from a spin spiral with $\mathbf{q} = \frac{2\pi}{a}(0.8, 0.8, 0)$ without the inclusion of spin–orbit coupling to $\mathbf{q} = \frac{2\pi}{a}(1, 1, 0)$ when the spin–orbit coupling is considered. The latter corresponds to a Fe lattice with a type G antiferromagnetic ordering and a ferromagnetic U lattice, close to the ground state configuration previously determined. This result illustrates the importance of spin–orbit coupling in determining the ground state magnetic configuration of UFe_4Al_8.

In order to evaluate the accuracy of the *frozen spin–orbit coupling* approach, calculations with the propagation vector $\mathbf{q} = \frac{2\pi}{a}(0.8, 0.8, 0)$ and spin–orbit coupling terms corresponding to different directions of the U moment relative to the crystal axis were also performed. The results of this test are represented as the various points for $\tau = 0.8$ in figure 5: the energy differences of these configurations are more then one order of magnitude smaller them the energy variation with τ, which leads to the conclusion that the results presented in figure 5 are a clear indication of the variation of the energy of a configuration with the propagation vector. Furthermore, in order to identify the role of the *relative* orientation between the U and the Fe moments, another series of calculations was performed with both lattices constrained to the cycloid with $\mathbf{q} = \frac{2\pi}{a}(0.8, 0.8, 0)$, but with the introduction of an additional phase difference between them, ψ. Thus the angle between the atomic moments, θ, is given by $\theta = \mathbf{q} \cdot (\mathbf{r}_{Fe} - \mathbf{r}_U) + \psi$. Results show that the change in energy due to the change of

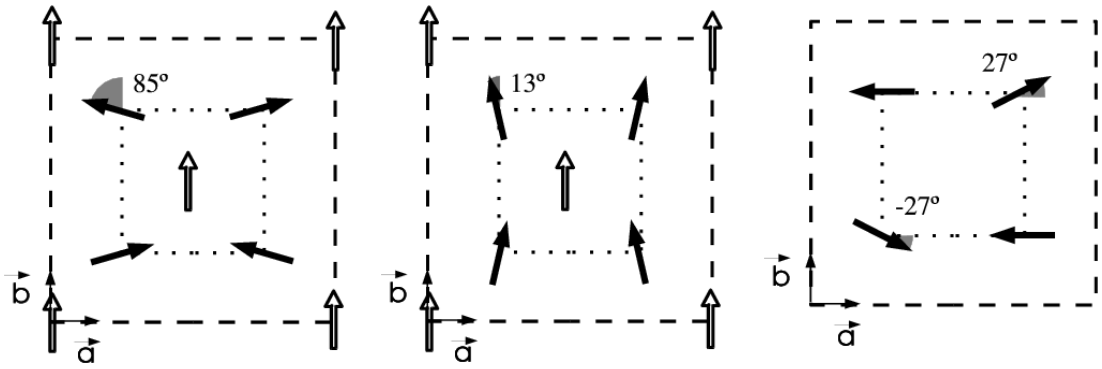

Figure 6. Projection of the Fe (black arrows), U and Np (white arrows with black borders) magnetic moments in the **a**–**b** plane, for, from left to right, UFe_4Al_8, $NpFe_4Al_8$ and YFe_4Al_8.

the *relative* orientation is again small when compared with the changes due the variation of τ in the propagation vector $\mathbf{q} = \frac{2\pi}{a}(\tau, \tau, 0)$, of the order of 0.1 mRyd. This shows that the phase between the U and Fe cycloids is not determinant for the lowest energy magnetic configuration. In the absence of spin–orbit coupling YFe_4Al_8 and UFe_4Al_8 form a spin spiral ground state with a propagation vector of $\mathbf{q} = \frac{2\pi}{a}(0.8, 0.8, 0)$ (for U) or $\mathbf{q} = \frac{2\pi}{a}(0.85, 0.85, 0)$ (for Y) has a lower energy than the type G antiferromagnetic Fe ordering. Including spin–orbit coupling in the UFe_4Al_8 calculation impedes the formation of this spin spiral state. On the other hand, the magnitude of the Fe magnetic moments hardly changes for different magnetic configurations. The values are also in very good agreement with the experimental values.

The calculated ground state structures for all of these compounds have the Fe moment in a noncollinear configuration in the basal plane, corresponding to different variations of the type G antiferromagnetic ordering. Figure 6 shows the relative alignment of the magnetic lattices for these two compounds: to allow a further comparison between actinide/rare earth compounds, the structure for $NpFe_4Al_8$ is also shown. The spin spiral of YFe_4Al_8 can be seen as a deviation from an antiferromagnetic ordering by one of the two Fe sublattices. This deviation is of 24° according to neutron diffraction data [3], or 27° according to the calculations (figure 6). Thus the similarity between the magnetic structures of the Fe lattice of UFe_4Al_8 and YFe_4Al_8 is evident, both compounds have a Fe sublattice with a structure that corresponds to a deviation from a type G antiferromagnetic structure, deviation that is constrained by the different symmetry properties of each compound, as imposed by the differences in the spin–orbit coupling in the compounds. The magnitude of the actinide moment influences the orientation of the Fe moments: the higher the spin moment of the actinide the lower the angle between the two sublattices (figure 6 and table 4). The spin moment of Np is considerably higher than the U spin moment, which justifies the calculated angles for the Fe moments in $NpFe_4Al_8$ and UFe_4Al_8 and a test calculation with a zero Np moment results in a magnetic Fe structure that is very similar to that in the U compound.

Table 4. Calculated magnetic moments and experimental magnetization for the ground state structures of the three compounds YFe_4Al_8, UFe_4Al_8 and $NpFe_4Al_8$.

Atom	m_{spin} (μ_B/atom)	m_{orb} (μ_B/atom)	m_{total} (μ_B/atom)	M_{theory} (μ_B/fu)	M_{exp} (μ_B/fu)
YFe_4Al_8				0	0 [3]
Y	$\leqslant$0.1	$\leqslant$0.1	$\leqslant$0.1		
Fe	1.25	0.08	1.33		
UFe_4Al_8				0.6	1.6 [6]
U	−0.08	0.21	0.17		
Fe	1.33	0.07	1.40		
$NpFe_4Al_8$				5.5	2.3 [22]
Np	−3.33	3.20	−0.13		
Fe	1.37	0.07	1.44		

3.3. Calculation of the exchange constants for YFe_4Al_8 and UFe_4Al_8

Calculations based on the frozen magnon approximation [40] have been used to determine the exchange constants and the ordering temperatures for ferromagnetic YFe_2 and UFe_2 [42]. Although the absolute T_C values were not accurately reproduced, the calculated values reproduced the large difference in the values of T_C. Here we present a similar study performed for YFe_4Al_8 and UFe_4Al_8.

YFe_4Al_8 and UFe_4Al_8 are essentially antiferromagnetic with ordering temperatures of 185 and 153 K, respectively, with deviations from the antiferromagnetic configurations as described earlier. In order to study the influence of the magnetic ordering on the application of the frozen magnon approximation, we started with a detailed study of YFe_4Al_8, and calculate the transition temperature using different ferro and antiferromagnetic configurations. We considered spin excitations where the moment is deviated 30° from the axis of rotation, which corresponds to perturbations of the following magnetic configurations: ferromagnetic along **c**, ferromagnetic and antiferromagnetic along **a**. The total energy dependence with the propagation vector **q** was calculated for three independent directions, with the use of the *force theorem*. These energy curves were fitted using a sum over the terms $J_i(1 - \mathbf{R}_j \cdot \mathbf{q})$ for each site j of the coordination sphere i. The number of considered spheres is relatively high even for

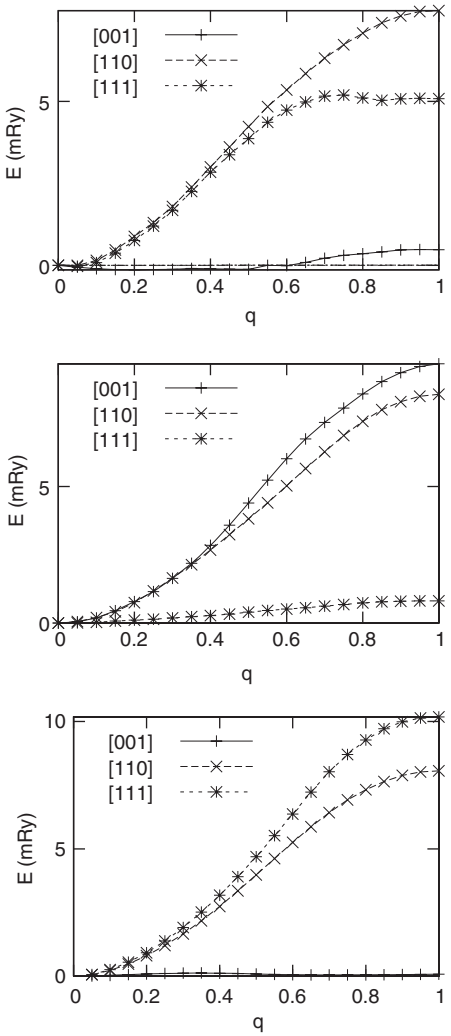

Figure 7. Calculated energy versus q calculated for three magnetic configurations with the moments along the **a** axis (symbols). The line corresponds to the fitting with the exchange constants in table 5. The magnetic configurations, from top to bottom, are: (1) YFe_4Al_8, ferromagnetic; (2) YFe_4Al_8, antiferromagnetic; (3) UFe_4Al_8, antiferromagnetic.

small distances since the crystal structure is tetragonal with two formula units in each unit cell. The exchange constants are found by minimizing the deviation between the fitted curve and the calculated energy values.

In the first series of calculations for YFe_4Al_8 8 coordinations spheres and a ferromagnetic configuration with the moments deviated from the **c** axis were considered. The next series were performed for the ferromagnetic and antiferromagnetic configurations with the moments along **a**. The transition temperature was calculated within the mean field approximation. In figure 7 the energy dependence with q, the propagation vector, is presented.

The exchange constants for the nearest neighbour, table 5, are larger than the value calculated for Fe [43, 44], however they decrease quickly with the distance between neighbours which results in a lower transition temperature than for pure Fe. The YFe_4Al_8 calculated temperatures are, for the three cases considered, higher than the experimental values, this is

Table 5. Exchange constants and transition temperatures, calculated for YFe_4Al_8 and UFe_4Al_8. Ferro and antiferromagnetic configurations along the **a** and **c** axes.

J	YFe_4Al_8			UFe_4Al_8
(mRyd)	FM ∥ **c**	FM ∥ **a**	AFM ∥ **a**	AFM ∥ **a**
J_1	1.681	1.684	−1.748	−1.915
J_2	−0.180	−0.237	−0.231	−0.243
J_3	0.169	−0.141	0.062	0.184
J_4	0.088	0.218	0.011	−0.048
J_5	−0.004	−0.039	0.012	0.170
J_6	−0.038			
J_7	0.002			
J_8	−0.003			
T_C (K)	353	392	437	450

expected in the mean field approximation [43]. The calculated transition temperature is higher for the configuration with the moments along the basal plane, which is in agreement with the fact that this is the easy magnetization axis. A similar increase occurs when one changes from the ferromagnetic to the antiferromagnetic configuration, which again is to be expected as the latter is closer to the ground state configuration.

For YFe_4Al_8, the Y moment is essentially zero and only the Fe–Fe interactions were considered. For UFe_4Al_8, the U–Fe interactions were not considered since the U moment is induced by the Fe moment [11] and therefore it is the Fe lattice that determines the transition temperature. Both the exchange constants and the transition temperature have slightly larger values than the ones calculated for YFe_4Al_8. However the difference in the temperature is only of 3%, with values of 437 K for YFe_4Al_8 and 450 K for UFe_4Al_8. The experimental ordering temperatures are also relatively close, 185 and 153 K, respectively.

These results show that this method is not adequate for determining the exact temperatures, but that it reproduces the relation between the transition temperatures for the Y and U compounds where it is the Fe sublattice that determines the magnetic behaviour.

4. Conclusions

The magnetic behaviour of the compounds studied in the present work is determined by the Fe sublattice. The Fe moments have similar magnitudes in the compounds, 1.3 μ_B/Fe, independently of the ordering to which the sublattices were constrained in the calculations. As shown in figure 6, the calculated ground state structures for all the compounds have the Fe moment in a noncollinear configuration in the basal plane, corresponding to different variations of the type G antiferromagnetic ordering. For the actinide compounds, the application of the *frozen spin–orbit coupling* approximation is shown to be reliable and allow an analysis of 'spin spirals' in an actinide compound. The strong spin–orbit coupling makes the formation of spin spirals energetically unfavourable and the ground state configuration is a ferromagnetic actinide sublattice with the spin moment along one of the basal plane axes and a canted Fe sublattice that deviates from this direction.

The similarity between the magnetic structures of YFe_4Al_8 and UFe_4Al_8 is further emphasized by calculations for UFe_4Al_8 without spin–orbit coupling, where the ground state is found to be a spin spiral with a propagation vector of $\mathbf{q} = \frac{2\pi}{a}(0.8, 0.8, 0)$, very similar to that of YFe_4Al_8. The calculations for the compounds YFe_4Al_8 and UFe_4Al_8 and also for $NpFe_4Al_8$ are in good agreement with the experimental results and show common features, which can be summarized by the fact that all three Fe sublattices represent deviations form the G type antiferromagnetic, the determinant role of the Fe lattice in the basic magnetic behaviour, the role of spin–orbit coupling and the relation between magnitude of the moment of the M sublattice and the direction of the Fe moments. The identification of two different solutions for self-consistent calculations for UFe_4Al_8 explains the unusual results that were identified in a previous theoretical study.

We also present results for the exchange constants and critical temperatures of YFe_4Al_8 and UFe_4Al_8 calculated within the frozen magnon approximation. Calculations find that the Fe–Fe exchange constants and deduced transition temperatures are similar for these two compounds, reproducing well the relation between the experimental values, and indicate that the role of the U sublattice is comparable to that of the non-magnetic Y sublattice.

Acknowledgments

This work was initiated with financial support FCT/POCTI/35338/FIS/2000 co-funded by the European Community FEDER.

References

[1] Cardoso C, Sandratskii L M, Gasche T and Godinho M 2002 *Phys. Rev.* B **65** 94413
[2] Cardoso C, Sandratskii L M, Gasche T and Godinho M 2003 *Phys. Status Solidi* **236** 544
[3] Schobinger-Papamantellos P, Buschow K H J and Ritter C 1998 *J. Magn. Magn. Mater.* **186** 21
[4] Li H-S and Coey J M D 1991 *Handbook of Magnetic Materials* vol 6 (Amsterdam: Elsevier Science) chapter 1
[5] Sechovský V and Havela L 1998 *Handbook of Magnetic Materials* volume 11 (Amsterdam: Elsevier)
[6] Paixão J A, Langridge S, Sørensen S Aa, Lebech B, Gonçalves A P, Lander J H, Brown J P, Burlet P and Talik E 1997 *Physica* B **234–236** 614
[7] Kuznietz M, Gonçalves A P, Waerenborgh J C, Almeida M, Cardoso C, Cruz M M and Godinho M 1999 *Phys. Rev.* B **60** 9494
[8] Paixão J A, Ramos Silva M, Waerenborgh J C, Gonçalves A P, Lander J H, Brown J P, Godinho M and Burlet P 2001 *Phys. Rev.* B **63** 054410
[9] Récko K, Szymański K, Dobrzyński L, Satuła D, Suski W, Wochowski K, André G, Bourée F and Hoser A 2002 *J. Alloys Compounds* **334** 58
[10] Marques J G, Barradas N P, Alves E, Ramos A R, Gonçalves A P, da Silva M F and Soares J C 2001 *Hyperfine Interact.* **136** 333
[11] Sandratskii L M and Kübler J 1999 *Phys. Rev.* B **60** R6961
[12] Szymański K, Rećko K, Dobrzyński L and Satuła D 1999 *J. Phys.: Condens. Matter* **11** 6451
[13] Waerenborgh J C, Gonçalves A and Almeida M 1999 *Solid State Commun.* **110** 369
[14] Bonfait G, Godinho M, Estrela P, Gonçalves A P, Almeida M and Spirlet J C 1996 *Phys. Rev.* B **53** R480
[15] Bonfait G, Gonçalves A P, Spirlet J C and Almeida M 1995 *Physica* B **211** 139
[16] Godinho M, Bonfait G, Gonçalves A P, Almeida M and Spirlet J C 1995 *J. Magn. Magn. Mater.* **140–144** 1417
[17] Andreev A V, Nakotte H and Boer F R 1992 *J. Alloys Compounds* **182** 55
[18] Gal J, Pinto H, Fredo D, Shaked H, Schäfer W, Will G, Litterst F J, Potzel W, Asch L and Kalvius G M 1987 *Hyperfine Interact.* **33** 173
[19] Schäfer W, Will G, Gal J and Suski W 1989 *J. Less-Common Met.* **149** 237
[20] Gal J, Yaar I, Regev D, Fredo S, Shani G, Arbaboff E, Potzel W, Aggarwal K, Pereda J A, Kalvius G M, Litterst F J, Shäfer W and Will G 1990 *Phys. Rev.* B **42** 8507
[21] Schäfer W, Will G and Gal J 1991 *Eur. J. Solid State Inorg. Chem.* **28** (Suppl. S) 563
[22] Gonçalves A P, Almeida M, Cardoso C, Gasche T, Godinho M, Boulet P, Colineau E, Wastin F and Rebizant J 2005 *J. Phys.: Condens. Matter* **17** 909
[23] van der Krann A M and Buschow K H 1977 *Physica* B **86–88** 93
[24] Buschow K H and van der Krann A M 1978 *J. Phys. F: Met. Phys.* **8** 921
[25] Felner L and Nowik I 1978 *J. Phys. Chem. Solids* **39** 951
[26] Schobinger-Papamantellos P, Buschow K H J, Hagmusa I H, de Boer F R, Ritter C and Fauth F 1999 *J. Magn. Magn. Mater.* **202** 410
[27] Kalvius G M, Wagner F E, Halevy I and Gal J 2003 *Hyperfine Interact.* **151/152** 195
[28] Waerenborgh J C, Salamakha P, Sologub O, Gonçalves A P, Cardoso C, Sério S, Godinho M and Almeida M 2000 *Chem. Mater.* **12** 1743
[29] Cardoso C, Gasche T and Godinho M 2006 *J. Phys.: Condens. Matter* **18** 8817
[30] Stepien-Damm J, Baran A and Suski W 1984 *J. Less-Common Met.* **102** L5
[31] Florio J V, Rundle R E and Snow A I 1952 *Acta Crystallogr.* **5** 449
[32] Sikora W, Schobinger-Papamantellos P and Buschow K H J 2000 *J. Magn. Magn. Mater.* **213** 143
[33] Sandratskii L M 1998 *Adv. Phys.* **47** 91
[34] Eriksson O, Johansson B and Brooks M S S 1989 *J. Phys.: Condens. Matter* **1** 4005
[35] Kübler J 2000 *Theory of Itinerant Electron Magnetism* (Oxford: Oxford University Press)
[36] Liechtenstein A I, Katsnelson M I, Antropov V P and Gubanov V A 1987 *J. Magn. Magn. Mater.* **67** 65
[37] Brinkman W and Elliott R J 1966 *Proc. R. Soc.* A **294** 343
[38] Sandratskii L M 1991 *J. Phys.: Condens. Matter* **3** 8565
[39] Gasche T, Cardoso C and Godinho M 2004 unpublished
[40] Halilov S V, Eschrig H, Perlov A Y and Oppeneer P M 1998 *Phys. Rev.* B **58** 293
[41] Sandratskii L M and Bruno P 2002 *Phys. Rev.* B **66** 134435
[42] Sandratskii L M, Bruno P, Bergqvist L and Eriksson O 2003 unpublished
[43] Pajda M, Kudrnovský J, Turek I, Drchal V and Bruno P 2001 *Phys. Rev.* B **64** 174402
[44] Cardoso C 2005 *PhD Thesis* Department of Physics, Faculty of Science, University of Lisbon